

Journal of Materials Chemistry B

Accepted Manuscript



This is an *Accepted Manuscript*, which has been through the Royal Society of Chemistry peer review process and has been accepted for publication.

Accepted Manuscripts are published online shortly after acceptance, before technical editing, formatting and proof reading. Using this free service, authors can make their results available to the community, in citable form, before we publish the edited article. We will replace this *Accepted Manuscript* with the edited and formatted *Advance Article* as soon as it is available.

You can find more information about *Accepted Manuscripts* in the [Information for Authors](#).

Please note that technical editing may introduce minor changes to the text and/or graphics, which may alter content. The journal's standard [Terms & Conditions](#) and the [Ethical guidelines](#) still apply. In no event shall the Royal Society of Chemistry be held responsible for any errors or omissions in this *Accepted Manuscript* or any consequences arising from the use of any information it contains.

Sub-nanoscale free volume and local elastic modulus of chitosan/carbon nanotube biomimetic nanocomposite scaffold-materials

Cite this: DOI: 10.1039/x0xx00000x

Received 22th January 2015,
Accepted 00th XXX 201X

DOI: 10.1039/x0xx00000x

www.rsc.org/MaterialsBEneko Axpe,^{*a,b} Loic Bugnicourt^a, David Merida^b, Maite Goiriena-Goikoetxea^{b,d}, Iraultza Unzueta^{b,d}, Ruben Sanchez-Eugenia^e, Jose Angel Garcia^f, Fernando Plazaola^b and Sonia Contera^{*a}

Future progress in materials for tissue engineering and 3D cell cultures applications requires control of two key physical properties: nanoscale mechanical properties and mass transport. These requirements remain uncontrolled partly due to a lack of physical parameters and quantitative measurements. Using chitosan scaffolds as a model system in close-to-physiological conditions and a combination of experimental techniques and theory, we link structure with local nanomechanical properties. Additionally we introduce a parameter, the free volume, to predict variations in transport properties. By fabricating nanocomposites with single walled carbon nanotubes (SWNTs) we are able to test our approach: incorporation of acid-treated, soluble, ~80 nm SWNTs in a chitosan matrix leads to a 2 fold increase in mean local elastic modulus and a decrease of 3% of the free volume available for oxygen diffusion. Inclusion of hydrophobic, ~800 nm SWNTs leads to a 100 fold increase of elastic modulus and doubles the voids percentage available for the transport of glucose.

1 Introduction

Biomimetic porous structures based on nanostructured composite materials have emerged as promising candidates for drug delivery and tissue engineering applications. In the case of tissue engineering, biology and material science are combined for developing functional substitutes of tissues and organs¹. One of the strategies, is to mimic the capacity of extracellular matrix (ECM) to guide and control tissues with a synthetic material. *In vivo*, cells in tissues organize as a result of complex, dynamic, reciprocal chemical and physical interactions with the ECM, *e.g.*, cells sense and respond to the mechanical properties of the ECM.²⁻⁴ Diffusion of oxygen and nutrients are also regulated by the ECM.^{5,6} This control must be exerted on the nanometre scale as cell/matrix interactions mainly happen in that length range.⁷⁻⁹ Biopolymer nanocomposite scaffolds are considered as advantageous materials to engineer the multifunctionality of the ECM.¹⁰ Apart from structure and adhesion, there are two key physical requirements that must be fulfilled: controlled nanoscale mechanical properties⁷ and mass transport (*e.g.* nutrient perfusion and oxygen diffusion).¹¹ These conditions are not currently met; in fact mass transport has been identified as the most crucial pending challenge that hinders progress in tissue engineering.¹¹ The difficulty in controlling these properties lays partly on the lack of a suitable theoretical framework based on quantitative measurements of the relevant physical parameters.¹²

This paper has two main objectives: (i) to measure mechanical properties in physiological conditions at the nanometre scale and (ii) to identify and measure a physical parameter that can be directly

linked to theory that is able to predict mass transport properties of nanocomposite materials for tissue engineering.

In the case of mechanical properties, although nanoscale mechanical properties have been recognized to be crucial for tissue engineering materials,⁷ most published work reports on either bulk measurements of elasticity^{7,13} or nanoindentation studies on dry samples.¹⁴

Furthermore we propose the use of free volume theory to predict the transport properties of scaffolds used for tissue engineering and 3D cultures. Free volume theory has been used for decades in polymer physics to explain molecular transport properties.¹⁵ In this context, free volume holes inside a nanocomposite can be understood as subnanoscale free spaces between the polymer chains and the interface cavities between the polymer chains and the nanostructures.¹⁶ According to the free volume theory, molecular diffusion through interchain open spaces, or free volume holes, is necessary for transport.^{17,18} In other words, free volume in a polymeric material is necessary for diffusion of molecules through it. The molecular transport is determined by the thermodynamic state and the size of the free volume available for the migrating molecule. The free volume theory of diffusion has been successfully used for *e.g.* predicting gas transport properties in hydrated polymer electrolyte membranes for fuel cells.¹⁹ It has been demonstrated that fine-tuning of free volume in polymer matrices can be used to design and optimise gas transport properties in *e.g.* gas separation membranes.²⁰ Positron annihilation lifetime spectroscopy (PALS) is a unique technique capable of directly measuring sub-nanometre sized free volume holes and their distributions, even in biological systems.²¹ However, to our knowledge, these possibilities have never

been exploited for the design of biomimetic materials where transport is particularly important.

Free volume can also be related to mechanical properties of polymers and to interface phenomena.²² Experimental information linking the local mechanical, interface and structural properties of biomimetic scaffolds and the free volume voids inside them in physiological conditions is not available to the best of our knowledge.

Here we use chitosan as a model system that is widely used in tissue engineering applications because it is cheap, biodegradable, biocompatible, hypoallergenic, antibacterial, bioadhesive and can be molded to have interconnected high porosity.^{13,23,24} In tissue engineering, chitosan has been mainly used for scaffold of osseous tissues, as a promoter of cell growth and osteoconduction.^{25,26} To improve mechanical strength and the loss of structural integrity under wet conditions chitosan has been combined with other materials,²⁷ e.g. carbon nanotubes (CNTs).^{10,28-34} Chitosan/CNTs nanocomposites are biocompatible³⁴⁻³⁶ and antimicrobial.³⁷

To test the ability of our approach to detect differences, and to alter the design in order to tailor transport and mechanical properties, we introduce variations in the scaffold by fabricating biomimetic nanocomposites of chitosan with single walled CNTs (SWNTs) of different length and surface properties (hydrophilic vs. hydrophobic). Structures are characterized by scanning electron microscopy (SEM) and atomic force microscopy (AFM). The physical properties of chitosan scaffolds and chitosan SWNTs/nanocomposites are measured in solution, at controlled pH and ionic strength. (i) Using AFM nanoindentation we measure the local Young's modulus and the variations of moduli distribution and (ii) using PALS we measure, for the first time, the free volume hole sizes and distribution in close to physiological conditions of a biomimetic nanocomposite scaffold. Finally we predict transport properties for oxygen and glucose using free volume theory.

2 Experimental

2.1 Chitosan and chitosan/SWNT solutions preparation

Medium molecular weight chitosan (190 kDa – 310 kDa, 75 – 85 % deacetylated) and SWNT with a diameter size of 0.7 – 1.1 nm and a length of 300 – 2300 nm (mode 800 nm) (both from Sigma Aldrich, USA) were utilized. Acid-treatment of SWNTs was carried out by mixing 12.7 mg of SWNTs, 10 ml of sulfuric acid (Acros Organics) and 3.333 ml of nitric acid (Acros Organics) in a SFE 590/1 029050 ultrasound bath sonicator (Ultratreatedave Limited, UK) at 60 °C for 1 h. After this, the acid was filtered with a polytetrafluoroethylene (PTFE) filter for 24 h. Ultrapure water and 1 M NaOH was added to neutralize the acid on the nanotubes. The obtained solution was inserted in the ultrasonicator bath for 1 h. The resulting SWNTs had a length of 20 – 475 nm with a mean length of 78 nm (determined by AFM imaging).

50 mM sodium acetate buffer (Sigma Aldrich) containing 1% (vol) of acetic acid was prepared. The pH was adjusted to 4, using a 1 M NaOH (Sigma Aldrich) solution. 100 mg of chitosan powder (Sigma Aldrich) were added to 10 ml of the buffer in a round-bottom flask. The mixture was stirred with a magnetic shaker for 3h at 45 G. Next, an ultrasonicator bath (SFE 590/1 029050 Ultratreatedave, UK) was employed for 20 min. In order to remove undissolved chitosan, a centrifuge (5415D Eppendorf, Germany) was used for 5 min at 16,600 G. The supernatant was used for preparing 3 different samples: (i) 0.5 % wt chitosan solution was prepared by diluting with buffer the original solution. The obtained solution was stirred for 1 h at 33 G and then ultrasonicated for 30 min. (ii) 0.5 % wt

chitosan solution containing 0.25 mg/ml acid-treated SWNTs. The solution was stirred for 1 h at 33 G and transferred to an ultrasonicator bath for 30 min. (iii) 0.5 % wt chitosan solution containing 0.25 mg/ml “untreated” SWNTs was prepared. The solution was stirred for 1 h at 33 G and transferred to an ultrasonicator bath for 30 min. A VCX 400 probe ultrasonicator (Sonics & Materials Inc. Vibra Cell (USA)) was used to disperse the SWNTs. The power was set at 100 W for 1 h, until the sample was homogenized, in pulsing mode (0.8 s on, 0.2 s off). Finally, residues were removed by centrifuging the solution for 20 sec at 9,300 G.

2.2 Sample preparation for AFM imaging.

For imaging acid-treated SWNTs/chitosan complexes, a mixture of 1 ml (1 mg/ml) acid-treated SWNTs/chitosan, with 2 ml of chitosan solution (50 mM acetate/acetic acid buffer, pH 4) was prepared by shaking, resulting in good dispersion of the SWNTs. For imaging, the samples were further diluted to mg/ml. Then, a 0.5 µl drop was deposited on mica, rinsed with ultrapure water and air-dried. For images of untreated SWNTs/chitosan interactions 1 mg of untreated, dry, SWNTs were mixed with a 2 ml of chitosan solution by ultrasonication (100 W for 1 h, pulse mode 0.8 s on, 0.2 s off, and maintained at 5 °C). For imaging, the samples were further diluted to mg/ml. Then, a 0.5 µl drop was deposited on mica, rinsed in ultrapure water and air-dried.

2.3 Scaffold fabrication

Three samples of 200 µl of each solution were deposited in a cylindrical mould. The samples were pre-frozen in dry ice at -65 ± 5 °C for 30 min. Next, the samples were freeze-dried at -65 °C under vacuum at 70 mTorr (VirTis 420617, SP Industries Inc., USA). The resulting sponges were neutralized in a 1 M NaOH solution for 5 h. Then, the scaffolds were rinsed 4 times and incubated for 15 min in ultrapure water. Finally, the samples were dried over 48 h under vacuum at 10 mTorr using a desiccator (Kartell, Italy) connected to a vacuum pump (A65201903 Edwards, USA).

2.4 Scanning Electron Microscopy (SEM)

Samples were fixed by a double coated, 8 mm-wide, carbon conductive tape from Ted Pella, Inc. (USA) and sputter-coated with a gold layer. Images were obtained with a S4800 SEM from Hitachi (Japan).

2.5 Positron Annihilation Lifetime Spectroscopy (PALS)

In order to perform the dynamic nanostructural analysis under physiological conditions, the sponges were hydrated for PALS measurements with a 10 mM HEPES buffer containing 154 mM NaCl and pH 7.4 at 37 °C. An ORTEC (USA) fast-fast coincidence system was used, with two BC-422 plastic scintillators from Saint Gobain (USA) and two H1949-50 Hamamatsu (Japan) photo multipliers put in a vertical position (explained elsewhere²¹) inside of a FFD-1402 refrigerator purchased from Radiber S.A. (Spain). The resolution function was 270 ps. The temperature of the samples was maintained at 37.0 ± 0.5 °C by an 3508 programmable temperature control system (Eurotherm, UK) equipped with a variable SALICRU (Spain) power supply, a FIREROD® cartridge heater of 100 W by WATLOW EUROPE (Germany), and a PT-100 CS5 (I15) temperature sensor supplied from TC S.A. (Spain). The heater and temperature sensor were installed in a sample holder made of pure aluminium. The ²²NaCl positron source of about 15 µCi was purchased from PerkinElmer (USA), evaporated between

two Kapton foils of 7.5 μm from CS Hyde (USA) and sealed by a double sided Kapton tape from CAPLINQ (Canada). Positron lifetime spectra were collected with $\sim 2.5 \cdot 10^6$ counts/spectrum. Lifetime analysis was carried out by using the LT_polymers program.³⁸ After subtracting the source contribution (19.84%, 0.382 ns), three lifetime components were obtained from each spectrum. The longest-lived lifetimes exhibited distributions, and the values of these distributions were used as o-Ps components for free volume void size calculations. For that purpose, Tao-Eldrup model equation was used.^{39, 40}

$$\tau_{\text{o-Ps}}^{-1}[\text{ns}] = 2(\text{ns})^{-1} \left[1 - \frac{R}{R_0} + \frac{1}{2\pi} \sin\left(\frac{2\pi R}{R_0}\right) \right]$$

with $R_0 = R + \Delta R$, R being the estimated average free volume hole radius, and ΔR an empirical parameter fitted to be 1.66 \AA .³⁵ The average free volume void size was evaluated (within the spherical approximation) as,

$$V_f = \frac{4}{3} \pi R^3$$

2.6 AFM Force Spectroscopy and imaging

Static force spectroscopy measurements and AFM imaging were performed using a MFP-3D AFM from Asylum Research (USA). Force vs. distance measurements were conducted after thermal equilibration, under physiological ionic strength conditions, using the same buffer as for PALS experiments. 3 μl of this HEPES buffer was deposited on freshly cleaved mica (Agar Scientific, United Kingdom); after 5 min, the sample was deposited and hydrated with 200 μl of the same buffer. SiN cantilevers (OMCL-RC800PSA-W, Olympus, Japan) with a nominal spring constant of 0.38 N/m. Individual spring constants were calibrated for each experiment using the thermal method, and the velocity of the z-piezo was fixed (1 $\mu\text{m/s}$) for each force vs. distance curve. Around 100 force curves were used for determining the local Young's modulus of each sample, using the Oliver-Pharr model.⁴²

$$\frac{1 - \nu_{\text{sample}}^2}{E_{\text{sample}}} = \frac{1}{E_{\text{eff}}} - \frac{1 - \nu_{\text{tip}}^2}{E_{\text{tip}}}$$

assuming that the Poisson's ratio of the sample is $\nu_{\text{sample}} = 0.5$ as in previous studies with hydrogel-like samples.⁴³⁻⁴⁵ Corresponding to a silicon nitride tip, the tip's Poisson ratio and modulus are $\nu_{\text{tip}} = 0.5$ and $E_{\text{tip}} = 290$ GPa respectively. The physical meaning and calculation of the effective elastic modulus E_{eff} is thoroughly described by the Oliver-Pharr method;⁴² for calculating E_{eff} , we assumed the correction factors $\beta = 1.05$ ⁴⁶ and $\epsilon = 0.727$.⁴⁷ As the depth along which contact is made between the tip and the sample was different for each indentation, the indenter area was calculated for each curve. For this, the tip was defined as a perfect pyramid with an included angle of $\phi = 35^\circ$ given by the cantilever manufacturer. The force curve analysis was conducted using routines from Asylum Research (USA) based on IGOR Pro program, WaveMetrics Inc. (USA). To ensure validity of the measurements, experiments were done at different indentations ranging from 20 nm to 100 nm.

AFM imaging was done with the same AFM. For imaging in air Si, Olympus OMCL-AC240TS cantilevers were used and for

imaging in liquid, SiN, Olympus OMCL-TR800PSA cantilevers were utilized. Amplitude-modulation AFM (AM-AFM) images were performed in air and in liquid imaging. For untreated SWNTs/chitosan interactions we used dual AFM, where the first two eigenmodes of the cantilever are excited, the feedback is done on the first eigenmode's amplitude, and variations of second eigenmode's phase are used to show material properties' contrast.

3 Results and discussion

First, the scaffolds produced by freeze-drying solutions of chitosan, chitosan/acid-treated SWNT and chitosan/untreated SWNTs were imaged by SEM. Fig. 1 shows (a) chitosan-only sponges, which exhibit few and poorly connected pores. In contrast, Fig. 1 (b) acid-treated SWNTs/chitosan and Fig. 1 (c) untreated SWNTs/chitosan scaffolds show more porous structures. The acid-treated SWNTs/chitosan sample exhibits interconnected pores 150 μm and the untreated SWNTs/chitosan sample presents a wide distribution of interconnected pores 150 μm .

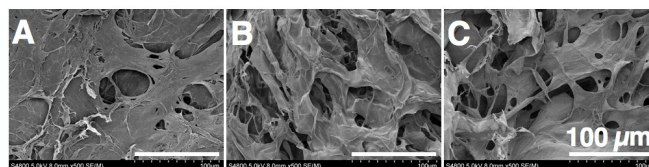


Fig. 1 SEM images of (a) chitosan, (b) chitosan/acid-treated SWNTs, and (c) chitosan/untreated SWNT nanocomposite scaffolds. The scale bar is 100 μm in all the images.

The interaction of individual SWNTs with chitosan macromolecules was studied using AFM imaging. First, AM-AFM imaging in liquid of chitosan molecules (not shown) confirmed that the height of individual molecules is 0.5 nm as in previous reports.⁴⁸ Fig. 2 (a) and (b) show the interaction of individual molecules of chitosan with 2 acid-treated SWNTs of different length; chitosan molecules seem to wrap around the SWNTs, dispersing them. Fig. 2 (c) shows a height image of longer, untreated SWNTs interactions with chitosan in air. The inset we show the phase contrast of the 2nd eigenmode of the cantilever in dual-mode AFM, which detects variations of materials mechanical properties,⁴⁹ identifying softer chitosan (darker grey) and stiffer SWNTs (lighter grey) and mica (white).

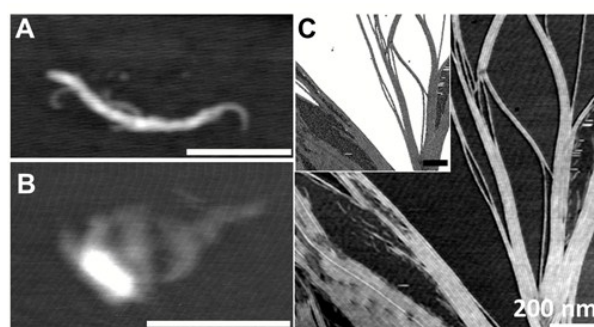


Fig. 2 AFM images of chitosan-SWNTs complexes. (a,b) AM-AFM height images of 2 individual acid-treated SWNT interacting with chitosan. The height scale is 0 - 2.5 nm (grey scale from back to white). (c) AM-AFM height image of the interaction of longer untreated SWNTs with chitosan molecules, the height scale is 0 - 2 nm. In the inset a 2nd eigenmode phase image in dual-mode shows mechanical properties contrast between the different materials (mica white,

SWNTs lighter grey, chitosan darker grey). The scale bar is 200 nm in all the images.

For determining the free volume hole sizes, the three scaffolds were immersed in buffer solution (10 mM HEPES buffer, 154 mM NaCl and pH 7.4 at 37 °C) for PALS experiments. The positron lifetime spectrum of a Ps-forming material typically includes three components due to short lived para-positronium, long lived ortho-positronium (o-Ps), and free positrons. The annihilation of o-Ps in polymers is dominated by the “pick-off” process in which the positron forming o-Ps annihilate with one of the surrounding spin opposite electrons. Tao and Eldrup constructed a successful theoretical model that relates the pick-off annihilation lifetime with the radius of the free volume hole using the equation described in Experimental section.

Positron lifetime spectra were collected with $\sim 2.5 \cdot 10^6$ counts for each sample. Obtained o-Ps lifetime distributions are shown in Fig. 3. The o-Ps mean lifetime are 1.87 ± 0.02 ns for chitosan, 1.80 ± 0.06 ns for acid-treated CNTs/chitosan, and 1.93 ± 0.02 ns for untreated CNTs/chitosan. Using the Tao-Eldrup equation we calculate the mean free volume void size and distributions shown in Table 1. The values for the acid-treated SWNTs/chitosan sample are respectively 6% and 28% shorter than in chitosan; conversely, for the untreated SWNTs/chitosan sample are respectively 6% and 20% larger than in chitosan alone.

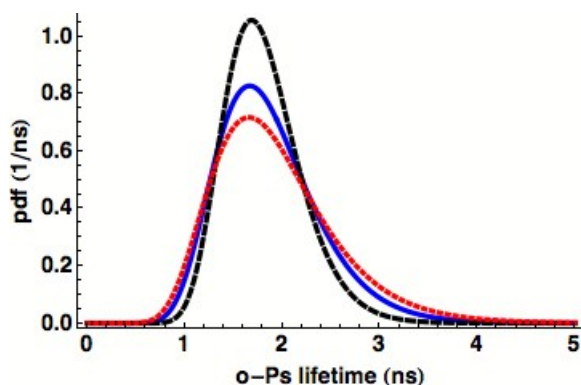


Fig. 3 Probability density functions (pdf) of lognormal distributions of measured ortho-Positronium (o-Ps) lifetimes corresponding to chitosan (blue), chitosan containing acid-treated SWNTs (dashed, black) and chitosan with untreated SWNTs (dotted, red).

	$\langle V_f \rangle [\text{\AA}^3]$	$\sigma [\text{\AA}^3]$	$\langle E \rangle [\text{kPa}]$	$\sigma [\text{kPa}]$
Chitosan	85 ± 2	50 ± 2	77 ± 3	26 ± 6
C/AT-SWNTs	80 ± 5	36 ± 2	171 ± 4	42 ± 8
C/U-SWNTs	90 ± 2	60 ± 2	8198 ± 283	2841 ± 566

Table 1 Mean free volume hole size ($\langle V_f \rangle$, \AA^3) and distribution (σ , \AA^3) obtained by PALS and mean Young's modulus ($\langle E \rangle$, kPa) and distribution (σ , kPa) obtained by AFM force spectroscopy in chitosan, chitosan containing acid-treated SWNTs (C/AT-SWNTs) and chitosan with untreated SWNTs (C/U-SWNTs).

For determining the local elastic modulus of the hydrated scaffolds in buffer solution, quasi-static force vs. distance nanoindentation measurements were performed using AFM in the same samples as the PALS experiments. The measured indentation curve is a function of the mechanical properties of the specimen, e.g. the elastic modulus. Typically, the extraction of properties is achieved by

applying a continuum scale mechanical model such as the Oliver Pharr. This methodology is in principle applicable to monolithic, isotropic materials. However, it has been shown that local properties of composites can be extracted from continuum analysis if the maximum indentation depth is smaller than the size of the embedded structures⁵⁰ (in our case SWNTs). It has been also demonstrated that the Oliver-Pharr method is applicable in nanocomposites if the indentation depth is smaller than the nanoparticle-dominated depth.⁵¹ In our experiments, maximum indentation depths (<100 nm) were chosen carefully for local modulus determination. Every indentation depth was much smaller than 10% of the sample thickness, and real contact areas were calculated one by one for each indentation. Given the aspect ratio of SWNTs and their interactions with chitosan, we can expect that our values arise from the local combination of the properties of both materials immersed in solution. These are in fact the values we are interested in, as the value and spread of those local variations would arguably be the most relevant parameters in the case of cellular attachment.

Fig. 4 shows histograms corresponding to the values of the Young's modulus for chitosan (a) chitosan containing acid-treated SWNTs (b) and chitosan with untreated SWNT (c) immersed in a physiological buffer solution, calculated using the Oliver-Pharr method as described in the Experimental section.

Comparison of (a) and (b) demonstrates that incorporation of short, acid-treated nanotubes in the chitosan leads to an overall increase of Young's modulus in around 100 kPa and a 15 kPa wider distribution of local modulus values. The effect of longer untreated (800 nm long) SWNTs in the chitosan matrix is more substantial, leading to an increase of about 100 times in mean value and a much larger distribution (over 10,000 kPa), arising from a more inhomogeneous zip structure due to the hydrophobicity of the untreated SWNTs reflected in AFM images. The width of the distribution is important and significant for tissue engineering and 3D cell culture applications, because it reflects the nanoscale variations that cells attaching to the scaffold would react to, as cells feel mechanical properties at the nm-scale, not the bulk elasticity, as mentioned in the Introduction.

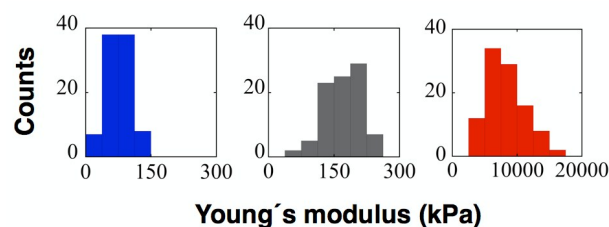


Fig. 4 Histograms corresponding to the values of Young's modulus for chitosan (blue), chitosan containing acid-treated SWNTs (black), and chitosan with untreated SWNTs (red). All the measurements are made in a HEPES buffer at 154 mM NaCl and pH 7.4. Note that the scale of the last histogram is wider than the rest.

Finally, using the free-volume probability density function from PALS, $V_{\text{pdf}}(V_f)$, we calculate the cumulative distribution of holes effective for transport C using the following relationship:⁵²

$$C(V_f \geq V_c) = \int_{V_c}^{V_{f,\text{max}}} V_{\text{pdf}}(V_f) dV_f$$

where $V_{f,\text{max}}$ is the largest free-volume hole of the material and V_c is the hole critical volume. Diffusion of a molecule in a homogeneous fluid system happens only when a free volume larger than certain critical size exists next to the molecule.⁵³ Free-volume voids smaller

than this critical size do not contribute to diffusion. Employing the Bondi's group contribution treatment,⁵⁴ the critical hole volume of the molecule can be estimated as $V_c = 1.3 V_w$, where V_c is the critical hole volume equal to the specific volume at absolute zero of the molecule, 1.3 is a factor assumed to be a universal constant effective for all groups and structures and V_w is the van der Waals volume of the diffusing molecule.

Free volume hole size distributions are plotted in Fig. 5. From these distributions, we calculated the cumulative distributions of holes effective for transport of oxygen and glucose, displayed in Table 2. The critical hole volumes were estimated ($V_{C,O_2} \sim 29.94 \text{ \AA}^3$ and $V_{C,C_6H_{12}O_6} \sim 252.55 \text{ \AA}^3$) using the Van der Waals radius and the bond length for oxygen and the molar mass and the density for the glucose respectively.

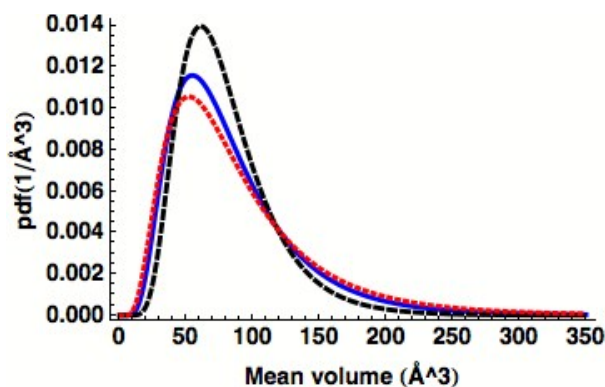


Fig. 5 Probability density functions (pdf) of free-volume hole size lognormal distributions corresponding to chitosan (blue), chitosan containing acid-treated SWNTs (dashed, black) and chitosan with untreated SWNTs (dotted, red).

	O ₂ (%)	C ₆ H ₁₂ O ₆ (%)
Chitosan	95.0 ± 0.7	1.2 ± 0.4
C/AT-SWNTs	98.1 ± 0.7	0.2 ± 0.2
C/U-SWNTs	93.5 ± 0.8	2.3 ± 0.3

Table 2 Estimation of the percentage of free volume holes available for oxygen (O₂) and glucose (C₆H₁₂O₆) diffusion obtained by PALS in chitosan, chitosan containing acid-treated SWNTs (C/AT-SWNTs) and chitosan with untreated SWNTs (C/U-SWNTs) hydrated scaffolds.

By introducing variations in the scaffold, i.e. fabricating chitosan nanocomposites with SWNTs, we are able to test the ability of our approach to detect physical differences and to tinker with the design to tailor transport and mechanical properties. As expected, incorporation of the different types of SWNTs in the chitosan scaffolds alters the conformation of the chitosan molecule, the structure, the free volume, the cumulative distribution of holes effective for transport and the local stiffness of the scaffold.

In the case of shorter, acid-treated SWNTs, the local nanoscale elastic modulus measured close to physiological conditions increases an order of magnitude. AFM imaging (Fig. 2 (a), (b)) suggests that the chitosan molecule wraps around individual SWNTs. Acid treatment of CNTs induces shortening and carboxylation of CNT defects and edges which facilitates their solubility in water, and non-hydrophobic interactions with biomolecules.⁵⁵ In the acidic medium used for the preparation of the complexes, chitosan chains are dispersed and can freely interact with SWNTs. In addition to

hydrophobic interactions, the presence of carboxyl groups at the edges and defects of SWNTs could provide electrostatic binding sites with the highly protonated ammonium groups present along chitosan chains at pH 4. This tighter molecular wrapping is consistent with the decrease in the mean free volume void size (which indicates a tighter packing of the biopolymer and the higher elastic modulus measured). This nanocomposite produces a better and more interconnected porous structure than chitosan alone (Fig. 1) with a pore size $\geq 150 \mu\text{m}$, which is suitable for e.g. bone tissue engineering applications.

Incorporation of longer, untreated SWNTs in the chitosan matrix produces a 2 order of magnitude increase in elastic-modulus and a much wider distribution. The porous structure of the scaffold and the different orientations of the SWNTs in the matrix could cause the larger spread of elastic modulus values. Interestingly, AFM imaging reflects a very different interaction of the chitosan molecules with the SWNTs (Fig. 2 (c)). Long SWNTs are *zipped-up* together by chitosan. In contrast with acid-treated SWNTs, untreated SWNTs are not soluble. The solubilization is caused by sonication with chitosan (see Experimental section). This process may induce stronger hydrophobic interactions, resulting in bundles of aligned SWNTs and chitosan molecules. The absence of defects at their surface would hinder the formation of electrostatic interactions with chitosan chains. The unzipping effect observed between some SWNTs in Fig. 2 (c) might result from the balance between hydrophobic and hydrophilic units along the polymer chains. While the N-acetyl-D-glucosamine unit of chitosan (hydrophobic part) would tend to bind to the SWNTs and form bundles, the hydrophilic part may induce repulsion between SWNTs after sonication. The ability of chitosan to solubilize SWNTs after sonication is due to the large proportion of hydrophilic groups along the polymer (Acetylation degree = 15 – 25%). While the hydrophobic part will wrap to SWNTs, the hydrophilic one would act like a stabilizing agent. The formation of complexes could also be possible through hydrogen bonding between the multiple hydroxyl groups all along the chitosan chains, these interactions should be weaker than hydrophobic interactions. The large increase in nanoscale elastic modulus measurements reinforces this interpretation, as bundles of longer SWNTs would be more difficult to deform than smaller, individually wrapped acid-treated SWNTs. PALS data show that the free volume void size is larger for a stiffer sample, which can be interpreted by an increased interfacial free volume.¹⁵ The presence of hydrophobic structures can be expected to increase the free volume in hydrated chitosan hydrogels.⁵⁶

Over the last decade, PALS has been employed to measure the size of the free volume holes in nanocomposites.⁵⁷ In this study, we provide for the first time PALS measurements of biomimetic nanocomposites immersed in a physiological buffer solution and we confirm that free volume void size and distribution can be determined by PALS in systems extensively used for cell culture^{21,58} employing chitosan-based scaffolds.

Using the free-volume probability density function from PALS, we calculate the cumulative distribution of holes effective for transport of oxygen and glucose. The results summarized in Table 2 highlight that the ratio of the free volume available for oxygen diffusion increases a 3% by incorporation of short acid-treated SWNTs to the chitosan scaffold. Incorporation of long, more hydrophobic, untreated SWNT, doubles the voids percentage available for the transport of glucose.

In recent years, measurements of diffusion in 3D cell cultures have received increased attention due to its importance for homeostasis^{6,59}. Crucially mass transport properties have been identified as the single most important issue preventing tissue engineering of complex tissues that can be used *in vivo* for replacing

damaged tissues or *in vitro* for e.g. drug testing¹¹. Arguably, one of the reasons why the transport problem remains unresolved is the lack of experimental parameters that can be used to link diffusion of molecules in cell-cultures with the scaffold physical properties. This link is important because it can lead to a rational design of the scaffolds that includes diffusion properties and hence it potentially facilitates the speed-up of the design and production of functional materials for cell culture. In polymer physics the concept of free volume has been successfully related to the diffusion of small molecules within the polymeric matrix.⁶⁰ Despite its demonstrated usefulness to explain and (more practically) to tailor diffusion⁶¹ in a system, free volume has never been invoked in the context of 3D cell cultures, homeostasis of tissues, biomaterial-mediated drug delivery or tissue engineering. Future experiments linking free volume with molecular diffusion in 3D cell cultures applications are necessary to validate this approach.

The combination of our experiments produces an intriguing result: small modifications of nanostructure, nanomechanics and local hydrophobicity can cause substantial free volume variations and interface effects. This, in turn, suggests an interesting speculation, namely that ECM in living tissues might be designed to optimize diffusion -in other words, free volume- and that hydrophobic components of the ECM such as elastin might be playing a fundamental role. This result should inspire future combined measurements of nanomechanical properties and free volume in ECM, ECM components and ECM-inspired systems.

4 Conclusions

We have introduced for the first time the concept of free volume in tissue engineering materials, and we have demonstrated that PALS can be used for measuring free volume void size and distribution of tissue engineering scaffolds in physiological conditions. When PALS is combined with structural and nanomechanical experiments, very valuable information about packing of the molecules and their interactions can be obtained. We have calculated the cumulative distribution of holes effective for molecular transport by using the free volume probability density function data obtained from the size and distribution of the free volume holes measured by PALS. By using nanocomposites of chitosan with SWNTs as a model system, we have shown that incorporation of acid-treated, soluble, ~80 nm SWNTs in a chitosan matrix leads to a 2 fold increase in mean local elastic modulus and a decrease of 3% of the free volume available for oxygen diffusion. Inclusion of hydrophobic, ~800 nm SWNTs leads to a 100 fold increase of elastic modulus and doubles the voids percentage available for the transport of glucose. In other words, our results show that the ratio of the free volume available for diffusion is modulated by the length and the surface properties of the SWNTs present in the nanocomposite scaffold.

Acknowledgements

Technical and human support provided by SGIker (UPV/EHU, MICINN, GV/EJ, ERDF and ESF) is gratefully acknowledged.

Notes and references

^a Clarendon Laboratory, Department of Physics, University of Oxford, OX1 3PU, Oxford, UK..

^b Department of Electricity and Electronics, University of the Basque Country UPV/EHU, Leioa, Basque Country, Spain.

^c Basque Center for Materials, Applications and Nanostructures, Parque Tecnológico Bizkaia, Derio, Basque Country, Spain.

^d Biofisika Unitatea, CSIC-UPV/EHU, Leioa, Basque Country, Spain.

^e Department of Applied Physics II, University of the Basque Country UPV/EHU, Leioa, Basque Country, Spain.

^f Department of Applied Physics II, University of the Basque Country UPV/EHU, Leioa, Basque Country, Spain.

* These authors contributed equally to this work.

Email: s.antoranzcontera1@physics.ox.ac.uk, eneko.axpe@ehu.eus.

- W. L. Murphy, T. C. McDevitt, and A. J. Engler, A. J., *Nat Mater*, 2014, **13**, 547-557.
- A. J. Engler, S. Sen, H. L. Sweeney and D. E. Discher, *Cell*, 2006, **126**, 677-689.
- F. Chowdhury, S. Na, D. Li, Y. C. Poh, T. S. Tanaka, F. Wang and N. Wang, *Nat Mater*, 2010, **9**, 82-88.
- P. M. Gilbert, K. L. Havenstrite, K. E. Magnusson, A. Sacco, N. A. Leonardi, P. Kraft, N. K. Nguyen, S. Thrun, M. P. Lutolf and H. M. Blau, *Science*, 2010, **329**, 1078-1081.
- D. M. Faulk, S. A. Johnson, L. Zhang and S. F. Badyal, *J Cell Physiol*, 2014, **229**, 984-989.
- T. Kihara, J. Ito and J. Miyake, *Plos One*, 2013, **8**, e82382.
- N. Huebsch, P. R. Arany, A. S. Mao, D. Shvartsman, O. A. Ali, S. A. Bencherif, J. Rivera-Feliciano and D. J. Mooney, *Nat Mater*, 2010, **9**, 518-526.
- P. Kanchanawong, G. Shtengel, A. M. Pasapera, E. B. Ramko, M. W. Davidson, H. F. Hess and C. M. Waterman, *Nature*, 2010, **468**, 580-U262.
- G. Maheshwari, G. Brown, D. A. Lauffenburger, A. Wells and L. G. Griffith, *J Cell Sci*, 2000, **113**, 1677-1686.
- T. Dvir, B. P. Timko, D. S. Kohane and R. Langer, *Nature Nanotechnol*, 2011, **6**, 13-22.
- E. C. Novosel, C. Kleinhan and P. J. Kluger, *Adv Drug Deliver Rev*, 2011, **63**, 300-311.
- M. Roussanova, D. J. Hughes, J. Enrione, P. Diaz-Calderon, E. Sivaniah, Q. Song, J. B. Ubbink, P. Beavis, A. C. Swain and M. A. Alam, *Acta Phys Pol A*, 2014, **125**, 801-805.
- W. W. Thein-Han, J. Saikhun, C. Pholpramoo, R. D. K. Misra and Y. Kitiyanant, *Acta Biomater*, 2009, **9**, 3453-3466.14 S. Chowdhury, V. Thomas, D. Dean, S. A. Catledge and Y. K. Vohra, *J Nanosci Nanotechnol*, 2005, **5**, 1816-1820.
- V. V. Volkov, *Polym J*, 1991, **23**, 457-466.
- G. Choudalakis and A. D. Gotsis, *Curr Opin Colloid In*, 2012, **17**, 132-140.
- S. Hong, *Ind. Eng. Chem. Res.*, 1995, **34**, 2536-2544.
- C. C. Hu, C. S. Chang, R. C. Ruaan and J. Y. Lai, *J Membrane Sci*, 2003, **226**, 51-61.
- H. Mohamed, Y. Kobayashi, C. S. Kuroda, N. Takimoto and A. Ohira, *J Membrane Sci*, 2010, **360**, 84-89.
- J. R. Wiegard, Z. P. Smith, Q. Liu, C. T. Patterson, B. D. Freeman and R. Guo, *J Mater Chem A*, 2014, **2**, 13309-13320.
- E. Axpe, T. Lopez-Euba, A. Castellanos-Rubio, D. Merida, J. A. Garcia, L. Plaza-Izurrieta, N. Fernandez-Jimenez, F. Plazaola and J. R. Bilbao, *PLoS one*, 2014, **9**, e83838.
- S. Napolitano and D. Cangialosi, *Macromolecules*, 2013, **46**, 8051-8053.
- F. Croisier and C. Jerome, *Eur Polym J*, 2013, **49**, 780-792.
- M. Dash, F. Chiellini, R. M. Ottenbrite and E. Chiellini, *Prog Polym Sci*, 2011, **36**, 981-1014.
- A. R. Costa-Pinto, R. L. Reis and N. M. Neves, *Tissue Eng Part B-Re*, 2011, **17**, 331-347.
- W. W. Thein-Han and R. D. K. Misra, *Mater Sci Tech Ser*, 2008, **34**, 1062-1075.
- C. M. Agrawal, J. L. Ong, M. R. Appleford and G. Mani, *Cambridge Texts in Biomedical Engineering*, 2013.
- L. Carson, C. Kelly-Brown, M. Stewart, A. Oki, G. Regisford, Z. P. Luo and V. I. Bakhmutov, *Mater Lett*, 2009, **63**, 617-620.
- I. Olivas-Armendariz, P. Garcia-Casillas, R. Martinez-Sanchez, A. Martinez-Villafane and C. A. Martinez-Perez, *J Alloy Compd*, 2010, **495**, 592-595.
- Y. L. Liu, W. H. Chen and Y. H. Chang, *Carbohydr Polym*, 2009, **76**, 232-238.

- 31 J. Venkatesan, Z. J. Qian, B. Ryu, N. A. Kumar and S. K. Kim, *Carbohydr Polym*, 2011, **83**, 569-577.
- 32 D. Depan, T. C. Pesacreta and R. D. K. Misra, *Biomater Sci*, 2014, **2**, 264-274.
- 33 W. W. Thein-Han and R. D. K. Misra, *Acta Biomater*, 2009, **5**, 1182-1197.
- 34 D. Depan, J. S. Shah and R. D. K. Misra, *Polym Degrad Stabil*, 2013, **98**, 2331-2339.
- 35 S. Pok, F. Vitale, S. L. Eichmann, O. M. Benavides, M. Pasquali and J. G. Jacot, *ACS Nano*, 2014, DOI: 10.1021/nm503693h
- 36 D. Depan and R. D. K. Misra, *J Biomed Mater Res Part A*, 2012, **100**, 3080-3091.
- 37 J. Venkatesan, R. Jayakumar, A. Mohandas, I. Bhatnagar, S. K. Kim, *Materials*, 2014, **7**, 3946-3955.
- 38 J. Kansy, *Nucl Instrum Meth A*, 1996, **374**, 235-244.
- 39 M. Eldrup, D. Lightbody and J. N. Sherwood, *Chem Phys*, 1981, **63**, 51-58.
- 40 S. J. Tao, *J Chem Phys*, 1972, **56**, 5499-5510.
- 41 H. Nakanishi, S. J. Wang and Y.C. Jean, *Positron annihilation studies of fluids*, World Scientific, 1988.
- 42 W. C. Oliver and G. M. Pharr, *J Mater Res*, 1992, **7**, 1564-1583.
- 43 K. Urayama, T. Takigawa and T. Masuda, *Macromolecules*, 1993, **26**, 3092-3096.
- 44 B. D. Johnson, D. J. Beebe and W. Crone, *Mat Sci Eng C-Bio S*, 2004, **24**, 575-581.
- 45 S. P. Marra, K. T. Ramesh and A. S. Douglas, *Mat Sci Eng C-Bio S*, 2001, **14**, 25-34.
- 46 W. C. Oliver and G. M. Pharr, *J Mater Res*, 2004, **19**, 3-20.
- 47 Y. H. Hu, J. O. You, D. T. Auguste, Z. G. Suo and J. J. Vlassak, *J Mater Res*, 2012, **27**, 152-160.
- 48 M. Kocun, M. Grandbois and L. A. Cuccia, *Colloid Surface B*, 2011, **82**, 470-476.
- 49 A. Gannepalli, D. G. Yablon, A. H. Tsou and R. Proksch, *Nanotechnol*, 2011, **22**, 355705.
- 50 G. Constantinides, K. S. Ravi Chandran, F. J. Ulm and K. J. Van Vliet, *Mater Sci Eng A*, 2006, **430**, 189-202.
- 51 W. Yan, C. L. Pun, G. P. Simon, *Compos Sci Technol*, 2012, **72**, 1147-1152.
- 52 H. L. Lv, B. G. Wang and Y. Kong, *Polym J*, 2009, **41**, 1049-1054.
- 53 D. Turnbull and M. H. Cohen, *J Chem Phys*, 1961, **34**, 120-125.
- 54 A. Bondi, *Physical Properties of Molecular Crystals, Liquids and Glasses*, Wiley, New York, 1968.
- 55 H. J. Burch, S. A. Contera, M. R. de Planque, N. Grobert and J. F. Ryan, *Nanotechnology*, 2008, **19**, 384001.
- 56 N. T. Tsui, A. J. Paraskos, L. Torun, T. M. Swager and E. L. Thomas, *Macromolecules*, 2006, **39**, 3350-3358.
- 57 T.C. Merkel, B. D. Freeman, R. J. Spontak, Z. He, J. Pinnau, P. Meakin and A. J. Hill, *Science*, 2002, **296**, 519-522.
- 58 S. Siles, G. Moya, X. H. Li, J. Kansy and P. Moser, *J Radioanal Nucl Chem*, 1999, **240**, 529-530.
- 59 A. Colom, R. Galgoczy, I. Almendros, A. Xaubet, R. Farre and J. Alcaraz, *J Biomed Mater Res A*, 2014, **102**, 2776-2784.
- 60 K. D. Yao, J. Liu, G. X. Cheng, R. Z. Zhao, W. H. Wang and L. Wei, *Polym. Int*, 1998, **45**, 191-194.
- 61 P. Neogi, in *Diffusion in polymers*. Marcel Dekker, New York 1996.

Graphical abstract

Nanoscale elastic modulus and mass transport properties calculated with free volume theory of biomimetic nanocomposite scaffolds for tissue engineering and 3D cell cultures applications.

